Challenges in estimating emissivity and surface temperature using flux tower measurements

Gitanjali Thakur[1,*], **Stanislaus J. Schymanski**[1,*], **Kaniska Mallick** [1], **Ivonne Trebs**[1], and **Mauro Sulis**[1]

[1]Luxembourg Institute of Science and Technology, ERIN, Belvaux, L-4422, Luxembourg
[*]gitanjali.thakur@list.lu
[*]stanislaus.schymanski@list.lu

ABSTRACT

Land surface temperature (LST) is a preeminent state variable that controls the energy and water exchange between the Earth's surface and the atmosphere. At the landscape scale, LST is derived from thermal infrared radiance measured using space-borne radiometers. At the plot-scale, the flux tower recorded longwave radiation components are inverted to retrieve LST. Since the down-welling longwave component was not measured routinely until recently, usually only the up-welling longwave component is used for the plot-scale LST retrieval. However, we hypothesize that ignoring reflected down-welling longwave radiation for plot-scale LST estimations may lead to substantial discrepancies compared to the approach including down-welling longwave radiation. This also has important implications for estimating the correct surface emissivity using flux tower measurements, which is needed for plot-scale LST retrievals. This study addresses in detail the consequence of omitting downwelling longwave radiation for LST and emissivity estimation. It uses observations at ten eddy covariance towers on different land cover types. We found that the LST values obtained using both up-welling and down-welling longwave radiation components (long equation) are 0.5 to 1.5K lower than estimates using only the up-welling longwave radiation components (short equation). Plot-scale emissivity was estimated using a fitting procedure based on observed sensible heat flux and estimated surface-to-air temperature difference. The emissivity obtained using the long equation was generally lower than if the short equation was used. We also quantified the uncertainty in plot-scale LST and emissivity estimates due to uncertainty in measured fluxes. We found that despite additional input data for the long equation, the uncertainty in plot-scale LST was not greater than if the short equation was used. Landscape-scale day-time LST obtained from satellite data (MODIS TERRA) were strongly correlated with our plot-scale estimates, but on average, higher by several Kelvin, regardless of the estimation method. For most sites, the correspondence between MODIS LST and plot-scale LST estimates increased significantly if plot-scale emissivity was used instead of the landscape scale emissivity obtained from satellite measurements. The results of this work have significant implications for the combined use of aerodynamic and radiometric measurements (which require plot-scale emissivity estimation) to understand the interactions and feedbacks between LST and surface-atmosphere exchange processes.

Introduction

The effects of global change are reflected in land surface temperature (LST) anomalies and their interannual variability[?]. It controls the magnitude and variability of the surface energy balance (SEB) components and simultaneously gets modulated by the SEB partitioning[?,?]. LST contains imprints of surface moisture and is extremely sensitive to evaporative cooling, which makes it a preeminent variable for studying evaporation and surface-atmosphere exchange[?,?,?]. It directly affects the amount of emitted longwave radiation and influences the saturation vapor pressure at the surface that drives latent heat flux. Thus, the ecohydrological functioning and carbon-water coupling are largely controlled by the surface temperature of the soil-vegetation system[?]. The availability of an extensive network of eddy covariance measurements (FLUXNET) allows us to understand the interactions and feedbacks between the surface-atmosphere exchange processes such as evaporation, transpiration, and its control by the atmosphere and vegetation at the diurnal time scale. However, the unavailability of direct LST measurements at the same scale hinders a detailed understanding of the interactions and feedbacks between LST and surface-atmosphere exchange processes, which is of utmost importance to the climate modeling community. In the last two decades, plot-scale radiometric data collected at eddy covariance sites (ECS) have gained popularity for in-situ LST retrieval due to its wide availability and high temporal resolution[?,?]. In addition to this, the LST estimates at plot-scale originate from a relatively homogeneous footprint in comparison to the satellite-derived LST (MODIS pixels). ECS measurements are primarily used to assess the impacts and feedbacks of climate change on key ecosystem fluxes[?]. By definition, LST is a thermodynamic temperature that can be felt or measured by an accurate thermometer at the land surface-atmosphere point-of-contact and is independent of wavelength[?]. The instantaneous value of LST is the result of interplay between the net radiation at the surface, ground heat flux (G), sensible heat flux (H) and latent heat flux (LE)[?]. Thus, LST can also be used for the estimation of H[?] and LE[?] between the surface and the atmosphere. LST provides the lower-boundary condition in SEB models for diagnostic estimates of LE and is highly relevant for drought monitoring[?,?,?]. Inversion of the longwave radiation in FLUXNET data to obtain LST has been found to strongly depend on the emissivity of the underlying surface[?], which is not available as routine measurement. Therefore, estimating in-situ LST is not straightforward due to the involvement of two unknowns (LST and emissivity) inside one measurement variable (up-welling longwave radiation). To circumvent this challenge, we conducted simultaneous retrievals of LST and emissivity by exploiting the longwave radiation components in conjunction with associated SEB flux measurements.

The SEB components can be sub-divided into radiative components (often lumped in net radiation, R_{net}) and thermodynamic components, including sensible, latent and ground heat flux (H, LE, G respectively):

$$R_{net} = H + LE + G \tag{1}$$

As the surface-to-air temperature difference drives the exchange of sensible heat between surface and atmosphere, all components of Eq. (1) depend on the LST. Net radiation (R_{net}) can be sub-divided into down-welling and up-welling components. Only a fraction of solar top-of-the-atmosphere radiation reaches the Earth's surface, as some is reflected back to space by clouds, some is absorbed by the atmosphere and emitted later as longwave radiation. The emitted longwave radiation as a function of surface temperature (T_s, K) and surface emissivity (ε) is given by Stefan-Boltzmann (SB) equation:

$$R_{lem} = \varepsilon\sigma T_s^4 \tag{2}$$

where σ (W m^{-2}K^{-4}) is the SB constant, ε is the surface emissivity ranging between 0 and 1, and T_s (K) is the LST. Emissivity is defined as efficiency of a surface to emit thermal energy relative to a perfect black body. For a land surface, it depends on soil type, vegetation cover, soil moisture, soil chemistry, roughness, spectral wavelength, temperature and view angle[?] Putting the radiative components together, we can sub-divide R_{net} into:

$$R_{net} = R_{sdwn} + R_{ldwn} - R_{sref} - R_{lref} - R_{lem} \tag{3}$$

Reflected shortwave in Eq. (3) is expressed as $R_{sref} = \alpha R_{sdown}$, where α is the surface albedo. Considering Kirchhoff's law, whereby the emissivity of a surface equals its absorptivity, emissivity values below unity result in reflected longwave radiation, expressed as:

$$R_{lref} = (1-\varepsilon)R_{ldwn} \tag{4}$$

LST or radiometric temperature is the "ensemble directional radiometric surface temperature"[?], and can be estimated from the infrared radiance emanating from a given surface with known emissivity[?]. The emitted and down-welling longwave radiance are measured at given angle within its instantaneous field of view (fov) by a downward facing sensor relatively close to the surface (a few meters for an eddy covariance tower). The radiation received by a pyrgeometer or infrared sensor is a combination of the radiation emitted and reflected by the surfaces in its fov.

$$R_{lup} = R_{lem} + R_{lref} \tag{5}$$

Substitution of Eqs. (4 and 2) into Eq. (5) yields R_{lup} as a function of emissivity, surface temperature and down-welling longwave radiation:

$$R_{lup} = \varepsilon\sigma T_s^4 + (1-\varepsilon)R_{ldwn} \tag{6}$$

Eq. (6) is then solved for LST as a function of measured longwave and known surface emissivity:

$$T_s = \sqrt[4]{\frac{R_{ldwn}}{\sigma} - \frac{R_{ldwn}}{\varepsilon\sigma} + \frac{R_{lup}}{\varepsilon\sigma}} \tag{7}$$

In order to invert LST as shown in Eq. (7), ε values are required. However, radiometers at ECS do not measure spectral bands separately to deduce emissivity directly. Therefore, we will deduce ε from observations of sensible heat flux (H), which is defined as the heat transfer driven by a surface-to-air temperature difference. It can be expressed mathematically in analogy to Ohm's law as:

$$H = \rho C_p (T_s - T_a)/r_a \tag{8}$$

where T_a (K) is the temperature of the air measured at a reference height above the surface, C_p (J kg^{-1} K^{-1}) is the specific heat capacity of air, ρ (kg m^{-3}) is the air-density, and r_a (s m^{-1}) is the total resistance to heat transport from surface to the atmosphere. In simplified form, we write:

$$H = m(T_s - T_a) \tag{9}$$

where m (m s^{-1}) is a proportionality constant (defined as $m = \rho C_p / r_a$ and broadly referred to as heat transfer coefficient) and depends on surface characteristics and micro-meteorology[?]. It is evident from Eq. (9) that for $T_s - T_a = 0$, H will be zero. This boundary condition and the linear relationship between H and ΔT has been used in the past to estimate ε at the plot-scale from observed H, T_a and estimated T_s using measured longwave radiation[?,?]. Another approach for plot-scale ε estimation filters the data where H is close to zero, substitutes T_s in Eq. (6) by T_a and solves for ε[?].

However, due to surface heterogeneity, sparse canopies are prone to footprint mismatch between the aerodynamic (flux tower) footprint and radiometric (hemispherical) footprint[?,?,?], where the aerodynamic footprint represents the area contributing to measured sensible heat and air temperature, while the hemispherical footprint is the area within the radiometer footprint, contributing to the measured longwave radiation (used for T_s estimation). This can result in a different boundary condition i.e. at $\Delta T = 0$, $H \neq 0$ as expressed in Eq. (10):

$$H = m(T_s - T_a) + c \tag{10}$$

where H is representative of the sensible heat flux from the eddy covariance tower footprint, T_s is representative of all the radiating surfaces in the radiometric sensor's view, and c is interpreted as the H from surfaces in the aerodynamic footprint that are not seen by the radiometer.

Plot-scale estimation of ε and LST using observed H, T_a, R_{lup} and R_{ldw} as described above and in the Methods section, may be prone to substantial uncertainty. It is unclear how uncertainties in observed fluxes propagate into the uncertainty of estimated LST and ε. By design, infrared thermal (IRT) sensors only measure up-welling infrared radiance and therefore cannot explicitly account for the amount of reflected down-welling infrared radiation in the signal. For a long time, down-welling longwave R_{ldw} was not routinely observed at ECS[?] and was also considered to be the most poorly quantified component of the radiation budget[?]. Therefore, the second term in Eq. (6) is commonly omitted, arguing that $\varepsilon \approx 1$, and therefore Eq. (6) is simplified to Eq. (2)[?]:

$$R_{lup} \approx \varepsilon \sigma T_s^4 \tag{11}$$

Eq. (11) can be solved for T_s to yield what we will term the "short equation" (seq) for T_s:

$$T_s \approx \sqrt[4]{\frac{R_{lup}}{\varepsilon \sigma}} \tag{12}$$

Note that the above derivation is actually flawed, as the second term of Eq. (6) was omitted arguing that $\varepsilon \approx 1$, and yet ε was retained in the first part of the equation. Nevertheless, even with the availability of down-welling longwave measurements[?], the use of Eq. (11) is still a common practice[?,?]. This gives rise to the question if the short equation (Eq. 12) is adequate to estimate LST from ground-based measurements. In the remainder of this paper, we will refer to LST obtained using the long equation (Eq. 7) as T_{leq} and to LST obtained using the short equation (Eq. 12) as T_{seq}.

To better understand and improve approaches of plot-scale LST estimation, the present study addresses the following research questions:

1. Can we obtain an adequate estimate of plot-scale LST while neglecting the reflected down-welling longwave radiation?

2. Does the estimation of plot-scale ε based on observed sensible heat flux (H) have an advantage over satellite-derived ε for plot-scale LST estimation?

3. How much uncertainty is introduced in plot-scale LST and ε due to uncertainty in measured EC fluxes?

To answer these questions, we analysed data for ten eddy covariance sites in different biomes and climates (see Table 2). Plot-scale broadband monthly emissivity was derived using observed H and estimated ΔT as proposed by Holmes et al.[?]. Plot-scale LST was estimated using plot-scale or landscape scale emissivity with (Eq. 7) and (Eq. 12). Plot-scale LST was compared with MODIS LST (TERRA satellite-sensed) for the times of satellite overpass. Uncertainty in ε and LST due to uncertainty in observed fluxes were calculated using SOBOL based uncertainty analysis (SAlib)[?]. See the Methods section for more details.

1 Results

1.1 Plot-scale ε using long and short equation

Following the method proposed by Holmes et al.[?,?], plot-scale monthly ε was estimated at the study site by fitting ε to minimise the root mean square error (RMSE) of the regression between H and $T_s - T_a$ (**SI Fig. 11**). In Fig. 1a, c, and d, we reproduced the original data of Figs. 2a, 3C, and 3Q from Holmes et al. (2009)[?] to validate our interpretation of their approach using the short equation (Eq. 12). We noted only marginal differences between the two results based on the short equation, which are likely due to different fitting algorithms. The replication of the $H(\Delta T)$ plot using the long equation (Eq. 7) with the same data is given in Fig. 1b and the time series of resulting ε values is shown in Fig. 1c, d, indicated by blue stars. The retrieved LST values were slightly higher when using Eq. (7) (compare a and b in Fig. 1). The use of the long equation (Eq. 7) resulted in substantially (10%) lower values of ε as compared to the values estimated by Holmes et al.[?] for the common study sites (Brookings, Fig. 1c and Yatir, Fig. 1d).

Another approach for plot-scale ε estimation (Maes et al. (2019)[?]) in combination with Eq. 7) resulted in even lower ε values for Brookings, as shown in Fig. 1c (red stars), whereas at Yatir, this approach gave an ε value higher than 1 (red star in Fig. 1d). Note that the long equation also yielded $H(\Delta T)$ relationship for many more months at Yatir Forest (blue star) than the short equation (black dots) as shown in Fig. 1d, as it resulted in achieving a strong correlation between H and ΔT (section 3 for details). The pattern of lower ε and higher LST using the long equation compared to the short equation was confirmed for all the ten sites used in the present study (Table **SI 2**).

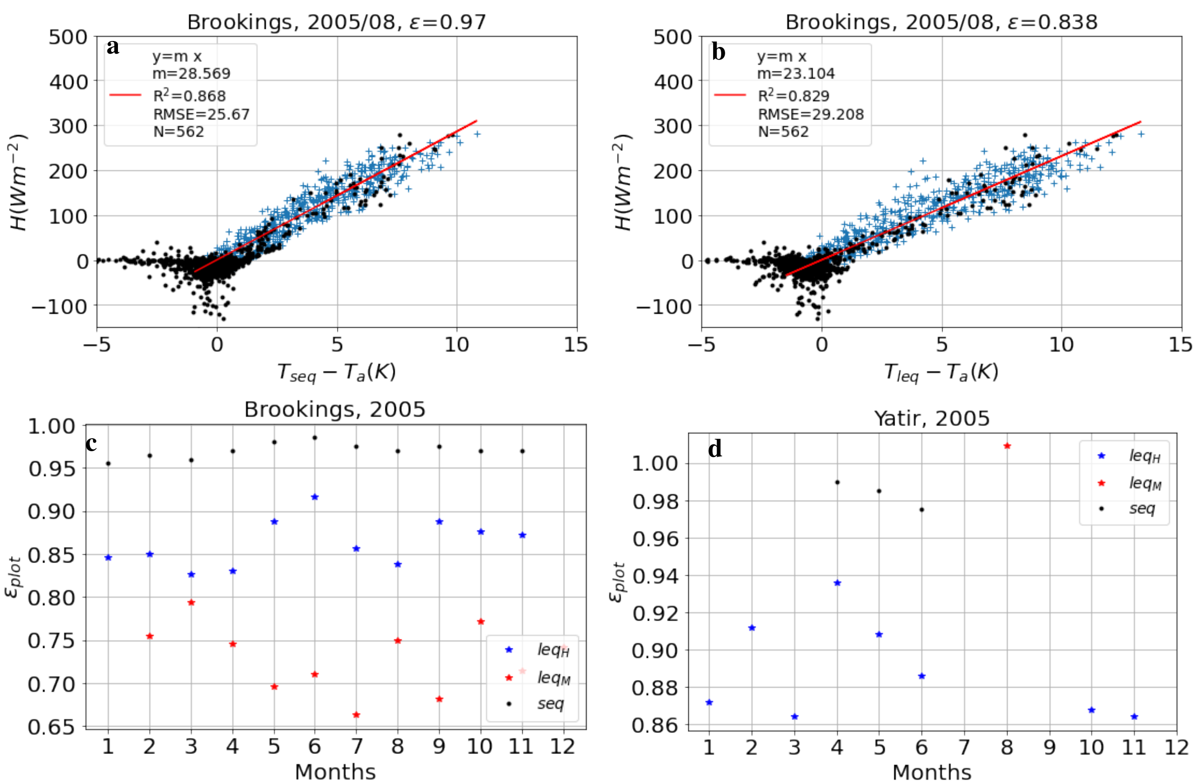

Figure 1. Reproduction of analysis presented in Figs. 2a, 3C, and Q in Holmes et al. (2009)[?]. **(a)** Sensible heat (H) vs. $\Delta T = T_{seq} - T_a$ based on the short equation (T_{seq}, Eq. 12); (b) H vs. ΔT based on the long equation (T_{leq}, Eq. 7). Both show data for August 2005 at Brookings. Blue crosses represent data points satisfying the filtering criteria, while black dots represent points not considered in the analysis. N is the number of blue crosses used for regression (red line), m is the slope of regression, RMSE is the root mean square error and R^2 is the square of the coefficient of determination. The fitted ε value is reported in the title. **(c)** Optimised ε values at Brookings obtained for the months where $R^2 > 0.5$ using the short equation (Eq. 11, black dots) and long equation (Eq. 6, blue stars), and ε obtained using the approach of Maes et. al (2019)[?] (red stars). **(d)** Same as (c), but for Yatir Forest, see table 2 for site descriptions.

1.2 Landscape scale vs plot-scale estimates of ε and LST

At each site, LST was estimated using both the short equation (T_{seq}, Eq. 12) and the long equation (T_{leq}, Eq. 7). In the first step, tower-based longwave radiation and landscape scale broadband ε from MODIS spectral ε (ε_{MODIS}, Eq. 14) was used.

The yearly daytime surface-to-air temperature difference for each study site is estimated and shown in Fig. 2. At all sites, Eq. (12) resulted in higher day-time plot-scale T_s estimates as compared to Eq. (7), when using ε_{MODIS}, with the medians of surface-to-air temperature differences (ΔT) differing by 0.8 to 1.5K (Fig. 2). The difference in ΔT using the two equations is highest at the water limited sites, e.g. AS and YA. Note that for two sites (LF and HS), the median values of daytime ΔT are negative. Comparison of estimated plot-scale LST using ε_{MODIS} at satellite overpass time with landscape scale LST (T_{MODIS})

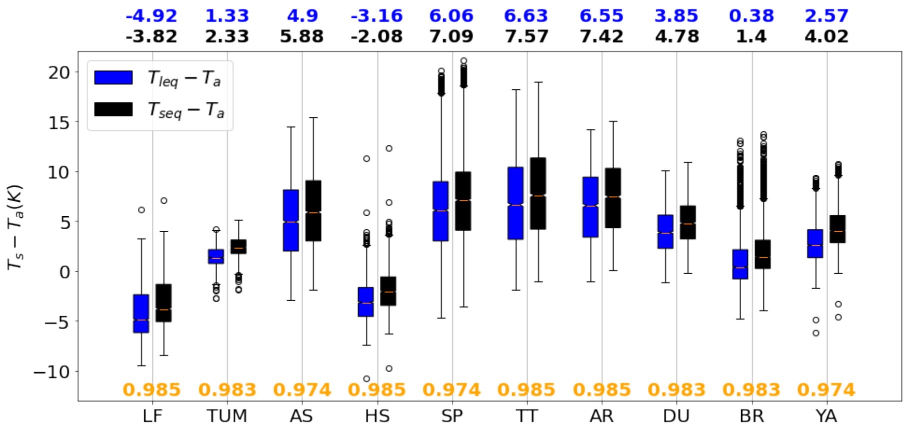

Figure 2. Yearly distributions of half-hourly surface-to-air temperature differences ($\Delta T = T_s - T_a$) for a representative year at each site. LST was calculated using the short or long equation (Eq. 12, Eq. 7) with landscape-scale emissivity (ε_{MODIS}). The median values of ΔT are shown at the top of the plot and the emissivities used for the T_s retrieval are shown at the bottom in orange. See Table 2 for site abbreviations.

revealed strong correlations between plot-scale and landscape scale LST estimates but systematically lower plot-scale LST (Fig. 3a, b). Use of plot-scale ε_{plot} for LST estimation (T_{seq} and T_{leq}) resulted in substantial reduction of the bias as shown in Fig. 3c, d. This trend in bias reduction was similar at other sites (Table **SI2** for details). The minimum bias is found at TUM, a closed canopy (eucalypt forest) and the highest bias was obtained at LF and HS, heterogeneous ecosystems with sparse canopies (woodland savanna). However, for some sites, weak correlation between satellite-derived and local LST estimates were also evident (at DU, R^2 was reduced from 0.8 to 0.4, see Table **SI2**). Also, using plot-scale ε for LST estimation resulted in positive $T_s - T_a$ at LF and HS as shown in **SI3, Fig. 8** in comparison to Fig. 2.

1.3 Plot-scale ε estimation considering intercept

In order to account for the possibility of bias between radiometric and aerodynamic measurements (e.g. due to footprint mismatch of measuring devices or instrument bias) we also fitted Eq. 10, i.e. a relationship allowing for an intercept in the linear fit between H and ΔT (instead of forcing it through zero as in Fig. 1) for plot-scale ε estimation. As shown in Fig. 5, the plot-scale ε values resulting from this approach ($H = m\Delta T + c$) were substantially closer to the landscape-scale ε values compared with the approach without intercept ($H = m\Delta T$), as shown in Table (1). The resulting intercept values ranged from -24 to +258 W m^{-2}, i.e. up to 70% of the maximum observed sensible heat flux at a site (e.g. at HS and TUM). Note, however, that if we assume just a slight under-estimation of upwelling longwave radiation by 40 W m^{-}2 (approx 8% of observed R_{lup}), the intercept at HS was reduced from 237 to 17 W m^{-}2 (Fig. 5a). In this study, we did not apply any energy balance closure scheme, as a Bowen ratio closure resulted in even greater intercept values (Fig. 5b). The comparison of the resulting plot-scale LST with landscape scale LST values reveals an increase in bias at most sites compared to the LST obtained using ε without an intercept, as shown in Table (1).

1.4 Uncertainty in plot-scale ε and LST

Each of the observed input variables used for the estimation of plot-scale ε and LST has a certain level of measurement uncertainty associated with it. Here we present exemplary results for Alice Springs, which showed the highest correlation between plot-scale and landscape scale LST estimations (Table 1).The uncertainty in plot-scale ε estimated using Eq. 7 ('leq') and Eq. 9 (i.e. without intercept in $H(\Delta T)$) was mainly in the range of ± 0.02 to ± 0.05, with a maximum of ± 0.2 if outliers are included (blue boxes in Fig. 6a). The short equation (Eq.12, 'seq') resulted in a vary narrow range of ε values between 0.94 and 0.99 throughout the year, with very small uncertainty (around ± 0.01, black boxes in Fig. 6a). Interestingly, the differences in ε uncertainty based on seq or leq did not propagate into differences in LST uncertainty, which were around ± 0.2 K at the hourly scale for each equations if plot-scale emissivity was used (blue boxes in Fig. 6b and black boxes in Fig. 6c). In fact, if landscape-scale values of ε were used, the uncertainty was even bigger (± 0.5 K, orange boxes in Fig. 6b and c).

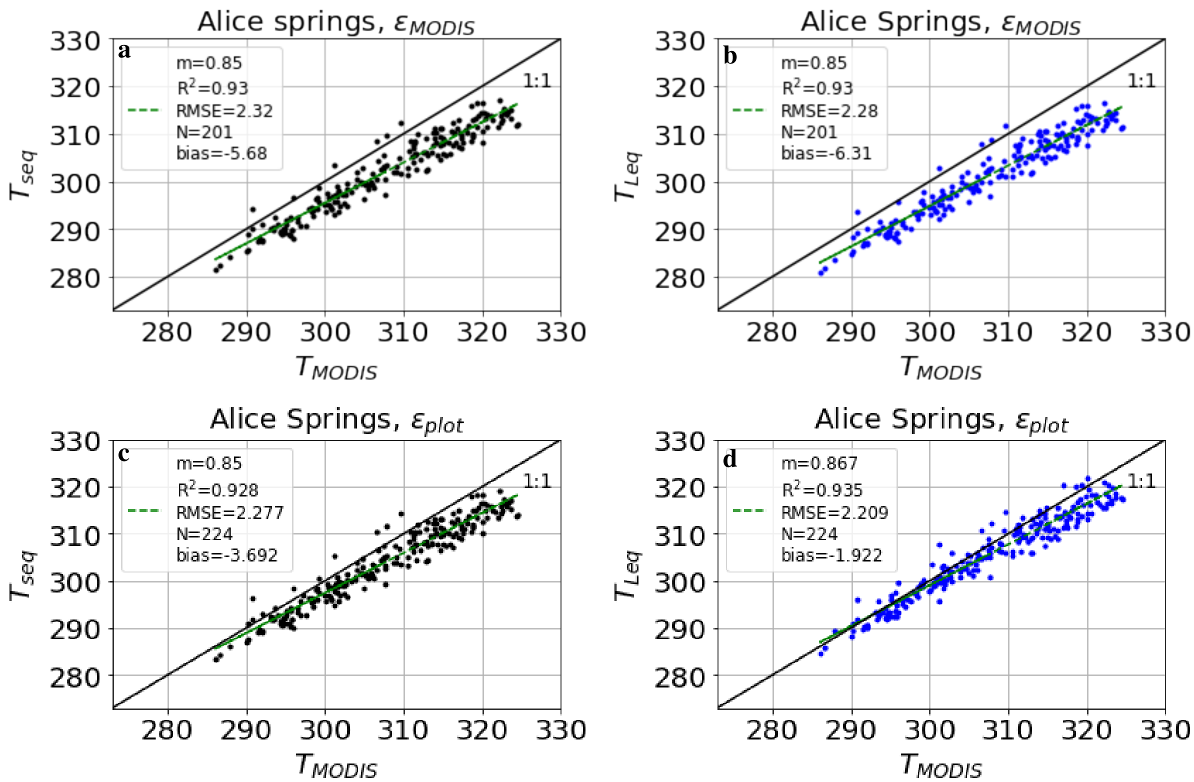

Figure 3. Landscape scale LST (T_{MODIS} derived from MOD11A1) vs. plot-scale LST at Alice Springs for 2016-2018. **(a)** T_{seq} based on short equation (Eq. 12) and satellite-derived (MODIS) broadband emissivity; **(b)** Same as (a), but T_{leq} based on long equation (Eq. 7); **(c)** T_{seq} based on short equation (Eq. 12) and monthly plot-scale emissivity; **(d)** Same as (c), but T_{leq} based on long equation (Eq. 7). Bias is mean $T_{seq} - T_{MODIS}$, N is the number of daily overpasses of MODIS between 2016 and 2018, c is the intercept, m the slope, RMSE is the root mean square error and R^2 is coefficient of determination. At each site, LST was estimated using both the short equation (T_{seq}, Eq. 12) and the long equation (T_{leq}, Eq. 7). In a first step, we used satellite-derived landscape scale broadband emissivity from MODIS (ε_{MODIS}, Eq. 14) for estimating plot-scale LST from tower-based longwave measurements, and compared these with landscape-scale LST extracted from MODIS LST dataset (T_{MODIS})

2 Discussion

Our analysis revealed a fundamental flaw in the commonly used short equation (Eq. 12) for estimating plot-scale LST and ε, as it does not produce the same results as the long equation (Eq. 7) even with high values of ε. In fact, the short equation strongly over-estimates the sensitivity of LST to ε (**SI Fig. 10**), as it neglects the fact that low emissivity results in a greater fraction of reflected longwave in the sensor signal (compare Eqs. 12 and 7). The sensitivity of the long equation (Eq. 7) to ε is driven by the contrast between R_{lup} and R_{ldwn}, whereas, for the short equation (Eq. 12), it is only driven by observed R_{lup} (**SI Fig. 9**). For instance, an error of 0.01 in ε at a water-limited site (e.g. AS) can cause an error of 0.17 K using Eq. (7) and 0.79 K using Eq. (12) respectively (**SI Fig. 10**). This means that small errors in ε can result in large differences in LST when using the short equation, or conversely, unrealistic LST values can conveniently be rectified by slightly changing the ε value. This is illustrated e.g. in Fig. 6, where estimation of plot-scale ε resulted in similar LST values between the short and long equations, but with vastly different ε values and much greater uncertainty in estimated ε using the long equation compared to the short equation. Considering that the short equation ignores an important component of longwave radiation, it must be concluded that in this case, it achieves seemingly the right results for the wrong reasons. The reduced sensitivity of the long equation (7) to ε is of advantage for plot-scale LST estimation, since plot-scale ε is usually unknown and therefore used as an approximate value[?].

However, when using the long equation in conjunction with plot-scale H measurements to estimate plot-scale ε, we obtained unrealistically low ε values at some sites (e.g. HS and LF, Table 1) in comparison to previously reported ε values for a soil-vegetation system[?,?]. This low bias in plot-scale ε estimates was largely removed if an intercept in the $H(\Delta T)$ relationship was allowed (right column in Table 1). The intercept (i.e. $\Delta T \neq 0$ at $H = 0$) could be caused by combining measurements coming from instruments (radiometer, eddy covariance system) with different footprints[?]. The mismatch of source areas

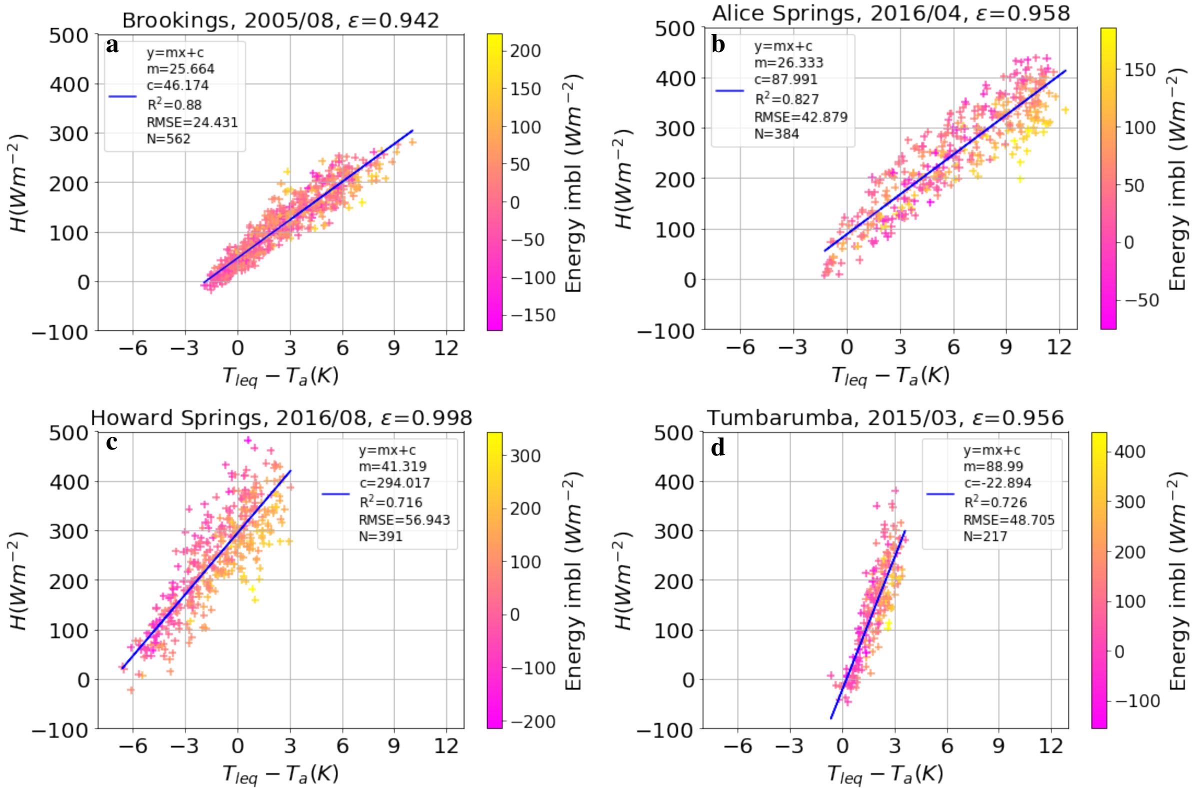

Figure 4. Sensible heat flux as a function of surface-to-air temperature difference based on Eq. 10 ($H = m(T_s - T_a) + c$). ε was fitted to minimise RMSE of a robust linear regression. The title of the plot contains site, year, month and the fitted ε-value. The legend correspond to Fig. 1. The colour code indicates the degree of energy imbalance of each data point (i.e. $R_{net} - H - LE - G$).

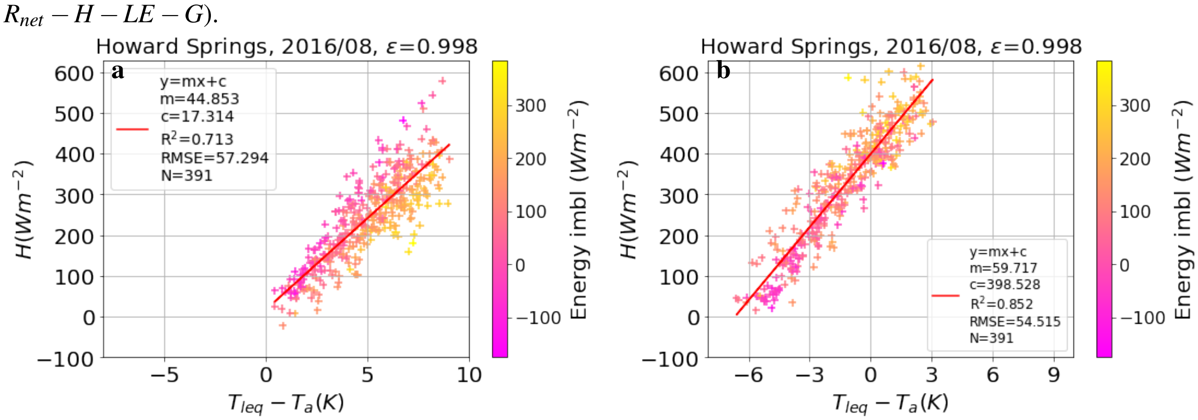

Figure 5. Sensible heat flux as a function of surface-to-air temperature difference based on Eq. 10 ($H = m(T_s - T_a) + c$). Same analysis and legends as in Fig. 5c), but (a) After adding 40 (Wm^{-2}) to measured R_{lup}, and (b) after closing the energy imbalance using a Bowen ratio closure scheme.

becomes important if the surface underlying the instruments has heterogeneous land cover. Although "footprint awareness" is often omitted at ECS under the assumption of homogeneity[?], in patchy vegetation, the radiation sensor can be "seeing" a different vegetation fraction than that contributing to EC measurements, meaning that $H \neq 0$ at $\Delta T = 0$. This problem was not detected by Holmes et al.[?], as the short equation (Eq. 12) was used, and due to its high sensitivity to ε (**SI Fig. 10** a) even a small reduction in ε corrected the offset in $H(\Delta T)$ (Fig. 1a). In contrast, when repeating the same analysis using the long equation (Eq. (7)), a larger reduction is required to remove the intercept, resulting in lower ε (Fig. 1b). By allowing an intercept in the $H(\Delta T)$ regression, we implicitly account for the possibility of a footprint mismatch or instrument bias in the data. This small change in methodology enables us to detect such problems by inspecting the value of the intercept (c). Considering the aerodynamic footprint to be larger than the radiometric footprint[?,?], a positive intercept can be interpreted

Sites	Landscape-scale ε			Plot-scale ε $H = m\Delta T$			Plot-scale ε $H = m\Delta T + c$			
	ε_{land}	R^2	bias (K)	ε_{plot}	R^2	bias (K)	ε_{plot}	R^2	bias (K)	c (Wm^{-2})
SP	0.974	0.81	-4.61	0.85	0.82	-1.91	0.92	0.774	-2.563	18.12
AS	0.974	0.93	-6.24	0.82	0.93	-1.92	0.993	0.915	-4.884	72.46
TT	0.974	0.57	-8.30	0.80	0.52	-4.02	0.939	0.521	-7.466	58.70
HS	0.985	0.16	-9.90	0.6	0.22	-2.47	0.949	0.18	-10.45	237.29
LF	0.985	0.41	-11.0	0.6	0.41	-2.57	0.968	0.378	-11.47	258
AR	0.985	0.27	-3.51	0.960	0.252	-2.98	0.996	0.27	-3.567	14.72
DU	0.985	0.81	4.61	0.985	0.425	-3.926	0.994	0.405	-4.603	-8.11
TUM	0.983	0.84	-2.10	0.97	0.89	-1.93	0.955	0.85	-1.696	-24.24
BR	0.983	0.937	-0.195	0.82	0.895	2.72	0.919	0.906	1.662	17.72
YA	0.974	0.855	-3.45	0.93	0.793	-0.582	0.873	0.826	0.073	-22.95

Table 1. Correspondence between daytime landscape-scale LST (T_{MODIS}) and plot-scale LST (T_s) (estimated at TERRA time of pass), using different emissivity estimates. The emissivity values used to retrieve plot-scale LST is either taken from MODIS (ε_{land}), or derived flux tower data (ε_{plot}), using Eq. 9 ($H = m\Delta T$) or Eq. 10 ($H = m\Delta T + c$). The reported ε_{plot} and intercept (c) are median values over all months for each site. Bias is defined as the mean of $T_s - T_{MODIS}$, R^2 is the coefficient of determination between plot-scale LST in comparison to landscape scale LST. The site acronyms are explained in Table 2.

as the H from the aerodynamic footprint which is not seen by the radiometer. The intercept was very high for sites like HS and LF (Table. 1). Placing high value of intercept into perspective for HS and LF, we looked closely at $H(\Delta T)$ plots for HS and LF (**SI** Fig. 8) and negative daytime $T_s - T_a$ (Fig. 2) we could hypothesize an underestimation of R_{lup}. Testing the hypothesis for HS (having high intercept, Fig. 5c) we found that adding roughly 40 Wm^-2 (approx 8% of observed R_{lup}, Fig. 12) in observed R_{lup} led to significant reduction in the intercept from 294 Wm^-2 (Fig. 5 c) to 17 Wm^-2 with positive $T_s - T_a$ as shown in Fig. 5a. The other linear regression parameter m, R^2, RMSE remained constant for Fig. 5a and Fig. 5c. The hemispherical view of the radiometers looking down at the heterogeneous canopy, makes it possible to have more tree crowns and less soil for HS and LF. This can lead to an underestimation of R_{lup}, approximately by 5-10% (**SI 6**, Fig. 12). Also, the offset in $H(\Delta T)$ was proportional to the maximum observed H for each month as shown in Fig. 5. The ratio between H_{max} and intercept varies between 0% to 30% for AS (**SI 7** Fig. 13). Previous studies have shown the dependence of footprint mismatch on wind direction[?,?,?] however we did not find and significant relation between intercept and dominant wind direction for each month. Surface heterogeneity has also been recognized as one of the potential causes for the lack of energy balance closure observed at most ECS[?,?] at diurnal scales. Therefore, as a prerequisite the observed turbulent fluxes are corrected using an energy balance closure scheme[?] before use. However, in our analysis the use of an energy balance closure scheme (based on Bowen ratio) led to much lower values of plot-scale ε using Holmes approach. Other studies on plot-scale ε estimation have also used the observed fluxes without correction[?,?,?,?]. The use of an energy balance closure scheme for plot-scale ε estimation led to an increase in positive intercept (sparse canopy, Fig. 5). We also looked into the intercept of $H(\Delta T)$ by closing energy imbalance using Bowen ratio closure scheme[?] which result into higher intercept as shown in Fig 5b. These results show that the relation between intercept in $H(\Delta T)$ and lack of energy balance closure is not conclusive.

Comparison of plot-scale LST with MODIS LST resulted into very high bias for sparse canopy which is in agreement with previous studies where the bias for sparse canopy reached upto $12K$[?]. Plot-scale LST estimates using plot-scale ε reduced the bias in comparson to MODIS LST as shown in Table **4**. The use of plot-scale ε also reduces the uncertainty in diurnal LST in comparson to landscape scale ε (Fig. 6b,c). However, LST estimated using plot-scale ε considering foot print mismatch ($H = m * \Delta T + c$) resulted into increase in bias for most of the study sites as shown in Table 1. The increase in bias could be attributed to implicit consideration of spatial heterogeneity (by accepting intercept) at plot-scale, whereas, MODIS LST (landscape scale) are integrated pixel information considering radiating signal from a homogeneous surface.

The fluxes observed at a soil-vegetation system is representative of the composite signal from both, soil and vegetation which typically have a different range of surface temperatures and emissivities[?]. The ε of soil strongly depends on soil moisture content[?], whereas, the ε of a canopy depends on its structural attributes and leaf area index, the latter of which varies strongly at the seasonal scale[?]. For example, the laboratory-measured directional ε for various canopy elements (bark, leaf and its arrangement, stem wood) ranged between 0.9 to 1[?]. Laboratory measurements of thermal infrared reflectance spectra suggests that the ε variation from structural unknowns, such as leaf orientation, is more significant than the differences in leaf component emissivity among plant species[?]. Consequently, it is clear that the ε of a surface is a function of many factors and detailed study of all these factors is out of scope of the present study. Thus, derivation of landscape-scale broadband ε_{land} from

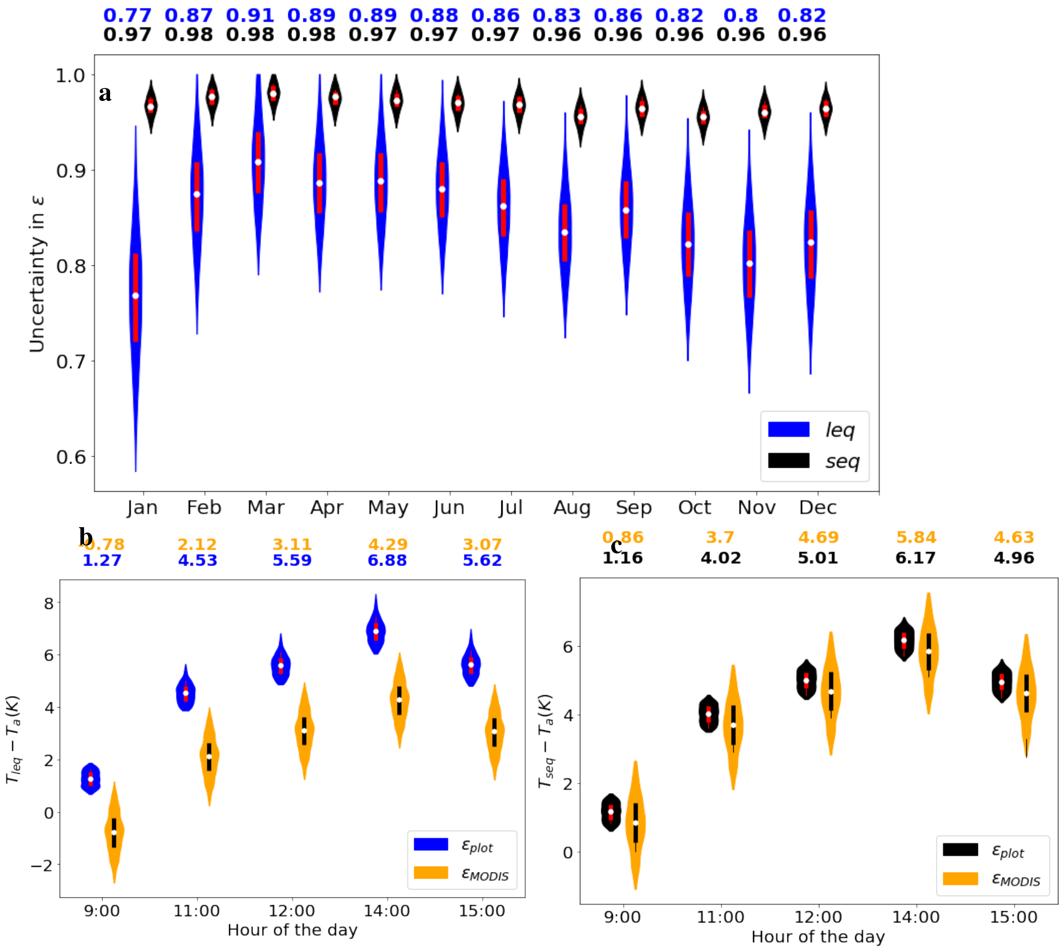

Figure 6. Uncertainty in plot-scale estimations of ε and surface-air temperature differences ($T_s - T_a$) at Alice Springs (AS), based on Eq. 9 (no intercept in $H(\Delta T)$). Monthly values of ε shown for 2017 and hourly $T_s - T_a$ for 15 August 2017. **(a)** Uncertainty in monthly plot-scale emissivity due to uncertainty in H, R_{lup}, R_{ldw} and T_a, using Eq. 6 ('leq', blue) and Eq. 11 ('seq', black). **(b)** Hourly uncertainty in $T_s - T_a$ based on Eq. 6, due to uncertainty in R_{lup}, R_{ldw} and T_a when landscape-scale emissivity is used (ε_{MODIS}, orange) or due to uncertainty in H, R_{lup}, R_{ldw} and T_a when plot-scale emissivity is used (ε_{plot}, blue). **(c)** Same as Panel b, but based on Eq. 11. Uncertainty calculated based on perturbations in input variables, where each box represents the median (red horizontal bar), 25% and 75% quantiles (filled bars) and range (whiskers) of output variables.

narrowband spectral emissivity is considered as a first-order approximation for capturing the integrated effects of land cover from MODIS spectral bands[?]. However, due to general lack of emissivity information for natural ecosystem at ECS, satellite derived emissivity serves as plausible estimates and are valuable input for plot-scale LST estimation. Plot-scale ε by fitting observed H and estimated ΔT without an intercept results into a lower value and is statistically questionable[?]. Since fluxes observed at ECS contain composite (soil and vegetation) signal aggregated over space and time therefore forcing $H(\Delta T)$ linear fit through zero is a simplification. Accepting an intercept in $H(\Delta T)$ linear regression gives a consistent slope to the curve which lead to reasonable representation of the observation at ECS further results into realistic range of ε_{plot}. Estimation of an intrinsic property like ε using time varying fluxes can be considered imprecise; however, considering the spatial and temporal limitation of satellite derived data, the plot-scale ε estimation is a good alternative.

Our results show that under no condition for grey bodies, the use of short equation and long equation can lead to equal values of ε and LST and thus, the use of Eq. (12) is not recommended. Considering the widely spread use of both ECS recorded fluxes and MODIS LST in LSMs applications, the use of plot-scale ε can be advantageous as it reduces the bias between plot-scale and MODIS LST. Plot-scale ε also lowers the uncertainty in diurnal LST due to measurement uncertainty in comparison to the MODIS based emissivity. Therefore, the approach proposed in this work has the potential to provide a more robust benchmark information for model calibration and validation. Realistic estimate of plot-scale ε by allowing an intercept in the linearfit of $H(\Delta T)$ emphasises on integration of "footprint awareness" concept for using eddy covariance fluxes. Overall, the implications of our study are of particular relevance for the research community interested in understanding diurnal and seasonal feedback in soil-vegetation systems based on fluxes, emissivity and LST estimated at a consistent scale.

3 Methods

3.0.1 Research data

Tower data: ECS collect micro-meteorological measurements above the surface (vegetation canopy) using towers (flux tower) following common measurement protocols[?]. The towers are commonly equipped with an instrument made up of pyrgeometers or radiometers to measure up-welling and down-welling shortwave and longwave radiation, which is further used to calculate net radiation (Eq. 3). Besides radiative fluxes, measurement at ECS also include sensible and latent heat fluxes, net carbon-dioxide exchange and a range of meteorological variables, such as air temperature, humidity and wind speed. T_a is the air temperature measured at a reference height above the canopy. Each flux measurement is accompanied by a flagging system based on the second CarboEurope-IP QA/QC workshop[?]. In our current work we use only high quality (flag 0) data. For the analysis, ten sites were selected to represent a variety of land cover types and climates (Table 2). Eight sites belong to the North Australian Tropical Transect (NATT) and two sites (Yatir Forest, Brookings) are chosen to replicate results from Holmes et.al[?]. Eddy covariance Level 3 data is obtained from http://data.ozflux.org.au/portal/pub/listPubCollections.jspx for Australian sites. The data for Brookings was obtained from ameriflux whereas the data for Yatir Forest was obtained from personal communication with Professor Yakir's lab in order to obtain the older version of the data which was used by Holmes et al.[?]

MODIS data: Landscape scale emissivity and LST data (MODIS product MOD11A1) was downloaded from NASA earth data . It is a level 3 daily LST product gridded in the sinusoidal projection at a spatial resolution of 0.928 *km* by 0.928 *km*. The daily LST pixel values in each granules (tile contains 1200 x 1200 grids in 1200 rows and 1200 columns) is retrieved by the generalized split-window algorithm under clear-sky conditions and MODIS LST values are averaged by overlapping pixels in each grid with overlapping areas as weight[?]. The downloaded data in hierarchical data format (hdf), were converted into tagged image file format (tiff) using a python package called PyModis[?]. From tiff the files are converted into csv format. The details of data extraction and conversion can be found at $https://renkulab.io/projects/gitanjali.thakur/modis_lst_fpar/$. Thermal remote sensing (MODIS) is used to measure spectral emissivity through four channels (28, 29, 30, 31) at wavelengths ranging between 8-12 μm[?] and the system of equations is iteratively solved for a given range of wavelengths (9 - 12μm) to obtain ε and LST using radiative transfer models[?,?,?] In the current study dataset columns used to compare plot-scale LST are: day time daily LST, local view time. In order to obtain landscape-scale the emissivity from bands 31 and 32 are used, these bands have more stable emissivities ranging from 0.92-1 thus used to derive broadband emissivity[?].

Plot-scale emissivity: This approach was initially proposed by Holmes[?] to estimate plot-scale ε using short equation with H, R_{lup}, T_a. In the present work, we have used both long equation (Eq. 7) and short equation (Eq. 12) to estimate ε. The prime variable used in the study are H, R_{lup}, R_{ldwn}, and, T_a while the ancillary variables R_n and wind speed (Ws) are used to filter the data for analysis. The data filtering criteria are ($R_n > 25Wm^-2$) and wind speed ($Ws > 2ms^-1$)[?]. Data($R_{lup}, R_{ldwn}, H, T_a$) satisfying the filtering criteria is segregated monthly. A predefined range of ε from 0.4 until 0.998 with a step size of 0.002 is used with longwave measurement (R_{lup}, R_{ldwn}) and T_s is estimated. For each month linear regression is performed between sensible heat (H) and surface-air temperature difference $T_s - T_a$ (Fig. 7b) using scipy $https://docs.scipy.org/doc/scipy-0.16.0/reference/generated/scipy.stats.linregress.html$. The monthly ε was obtained by applying condition such that $R^2 > 0.5$ and the RMSE is minimum. An illustration plot for RMSE and ε is shown in **SI5**. The ε is obtained for each month using both, long Eq.(7) and short equation Eq.(12) and termed as ε_{leq} and ε_{seq} respectively, as shown in Fig. 7b. In order to represent the true regression between observed H, and estimated $T_s - T_a$ at ECS, $H(\Delta T)$ linear fit is allowed to have an offset (intercept). Plot-scale ε was obtained for months where $R^2 > 0.5$ by minimising RMSE as explained before. For sites like HS and LF resulting into high value of intercept the 8% of day time observed R_{lup} was added to the measured data and monthly plot-scale ε was estimated. Additionally the energy imbalance at the study sites was closed using Bowen ratio closure scheme and the plot-scale emissivity was estimated.

Recently another approach for plot-scale ε estimation using Eq. (5) is discussed by Maes et.al (2019)[?]. For each month, the observed R_{lup}, R_{ldwn}, T_a are filtered for non rainy days, $-2 < H < 2$, and $\alpha < 0.4$. The ε is estimated by substituting $T_s = T_a$ in Eq. (5) as shown in Eq. (13). The monthly ε was represented as the median of ε obtained by substituting filtered data in Eq. (13).

$$\varepsilon = \frac{R_{ldwn} - R_{lup}}{R_{ldwn} - T_a^4 \sigma} \tag{13}$$

LST comparsion: LST estimates resulting into optimum ε for each month using linearfit with and without intercept $H(\Delta T)$ is compared to the MODIS daily LST. For each month the T_s estimates using plot scale $/epsilon$ and MODIS $/epsilon$ corresponding to exact TERRA daily time of pass was obtained (30 minute tower data was upsampled to each minute using linear interpolation). TERRA (satellite) overpasses at local solar time between 10:30 am to 12 pm in ascending mode[?].

Table 2. Description of study sites

Study site	latitute, longitude	Landcover	Time-period	longwave sensors	Sensor installation height (m)
Sturt Plains (SP)	-17.1507, 133.3502	Mitchell Grass	2016-2019	CG-2	4.8
Alice Springs (AS)	-22.2828, 133.2493	Mulga woodland, hummock grassland, river red gum forest	2016-2018	CNR1	12.2
Ti Tree East (TT)	-22.2870, 133.6400	Grassy mulga woodland, Corymbia/Triodia savanna	2016-2018	CNR1	9.9
Howard Springs (HS)	-12.4943, 131.1523	Open woodland savanna	2016-2018	CM-7B, CG-2	23
Litchfield (LF)	-13.1790, 130.7945	Tropical savanna	2016-2018	CNR4	31
Adelaide River (AR)	-13.0769, 131.1178	Savanna dominated by Eucalyptus tectifica and Planchonia careya	2006-2009	CNR1	15
Daly Uncleared (DU)	-14.1592, 131.3881	Woodland savanna	2016-2018	NRlite	21
Tumbarumba (TUM)	-35.6566, 148.1517	Wet sclerophyll	2015-2018	CM3 and CG3	70
Brookings (BR)	44.352, 96.840	Cropland	2005	pyrgeometers[?]	NA
Yatir Forest (YF)	35.052, 31.345	Evergreen needleleaf forest	2005	pyrgeometers[?]	NA

Plot-scale LST at local satellite overpass (T_{leq} and T_{seq}) was obtained using interpolated longwave radiation measurement and coressponding monthly plot-scale ε. Plot-scale daily LST is compared to MODIS LST in terms of mean, bias, RMSE and R^2 using a robust linear regression model (scipy stat model) as shown in Fig. 7a. The goodness of fit between plot-scale and landscape scale LST was determined by looking at R^2 as shown in Fig. 7b. The bias is estimated as mean of deviation between daily MODIS LST and ground based T_s ($T_{leq,seq} - T_{MODIS}$). See SI table for data sources and acronyms in **SI1**.

General approach: We estimate landscape scale broadband ε using MODIS spectral ε as shown in Bahir et. al (2017)[?].

$$\varepsilon_{MODIS} = 0.4587\varepsilon_{31} + 0.5414\varepsilon_{32} \tag{14}$$

Tower based longwave radiation measurement (R_{lup}, R_{ldwn}) passing the filtering criteria (as mentioned in site specific approach) along with MODIS based ε was used to invert LST using Eq. (7) and Eq. (12). The obtained plot-scale LST was compared to landscape scale MODIS LST using a robust linear regression as mentioned in site specific approach as shown in Fig. 7a.

Uncertainty estimation: In order to obtain the uncertainity in plot-scale $/epsilon$ due to systematic error (caused due to the bias in measurement devices) at the study sites. In a first step, based on the literature[?,?] the error bounds of each input variables (H, R_{lup}, R_{ldw}, T_a) used in plot-scale ε is defined. The error bounds for R_{lup} and R_{ldwn} are -5 to 5 W m^{-2}[?], for H, it is -20 to 20 W m^{-2} and for T_a, it is -1 to 1 K[?]. The error samples (perturbation) within bounds is generated using saltelli sampling scheme (using python based package name SALIB[?]). Each error sample is added to the monthly segregated measured fluxes as explained in site specific approach. Observed fluxes combined with perturbued fluxes are used to estimate T_s using Eq. (12)

and Eq. (7). The obtained range of diurnal T_s and observed T_a with perturbation is used to calculate the uncertainity in ΔT. Perturbed sensible heat flux($H + sampleerror$) and perturbed ΔT is used to obtain ε as described in site specific apporach. The range of monthly plot-scale $/epsilon$ obtained is reported as uncertainity in monthly ε.

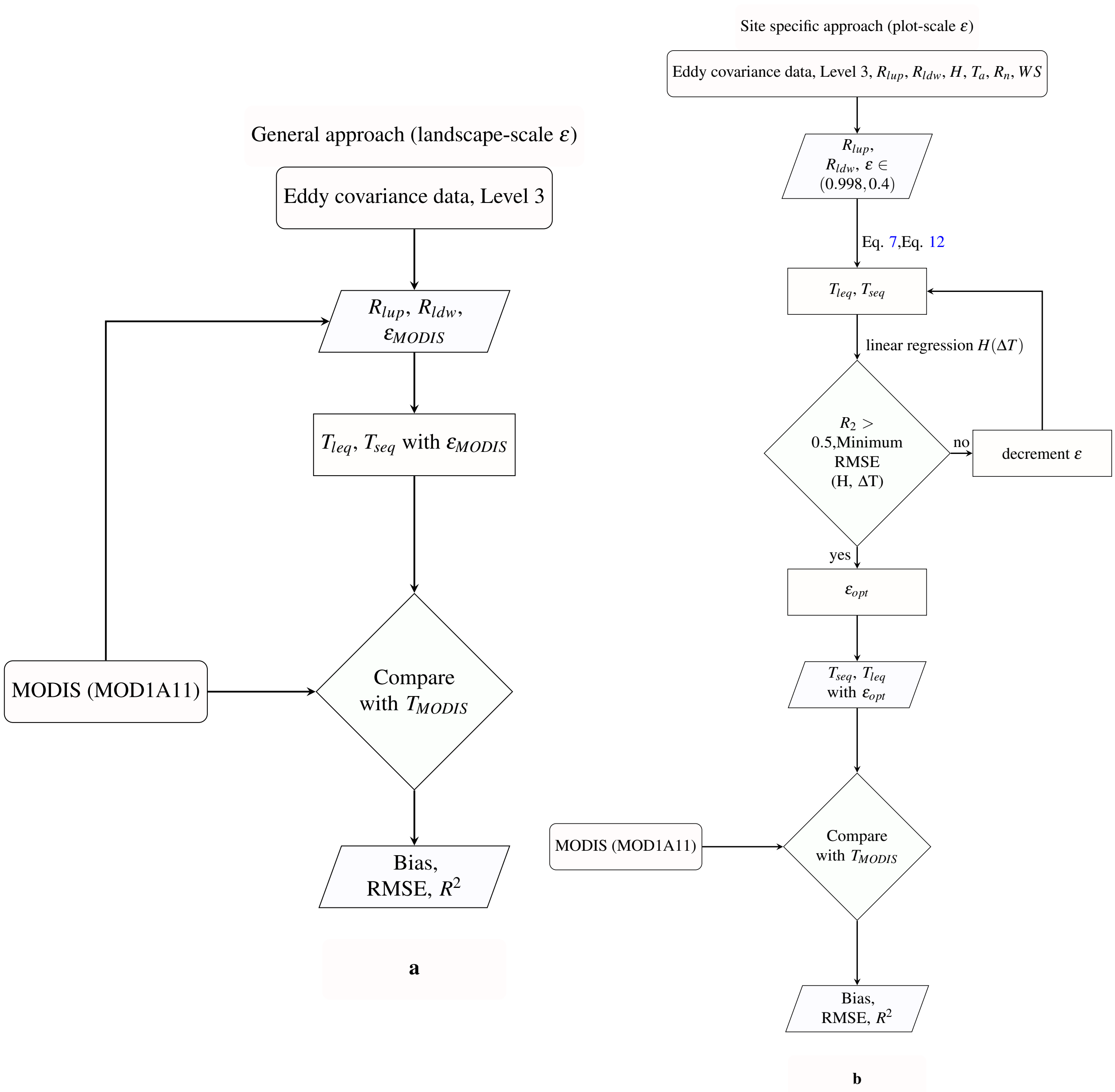

Figure 7. Schematic representation of steps followed for plot-scale LST retrieval using eddy covariance measurement (a) Landscape emissivity and longwave measurement and compared to Landscape-scale LST (T_{MODIS}) (b) Plot-scale emissivity estimation using observed H, R_{ldwn}, R_{lup} and plot-scale LST is estimated using plot-scale ε is compared to landscape-scale emissivity. The R^2, RMSE, Bias are mentioned in Fig. (3)

4 Acknowledgements

We would like to thank Dr. Maik Renner for pointing us to the work by Holmes et al. and Dan Yakir's lab for providing Yatir Forest data and helpful discussions. We are also grateful to Thomas Foken, Jason Beringer, Lindsay Hutley for insightful discussions and Remko Nijzink for his help in programming and RENKU. This work is supported by the Luxembourg National Research Fund (FNR) ATTRACT programme (WAVE, A16/SR/11254288). Mauro Sulis acknowledges the financial support of the FNR CORE programme (CAPACITY, C19/SR/13652816).

5 Supplementary Information

SI1. Abbreviation list

Table 3. Abbreviation list

Symbol	Description	Unit
R_{net}	Net radiation	W m^{-2} m
H	Sensible heat flux	W m^{-2}
LE	Latent heat flux	W m^{-2}
G	Ground heat flux	W m^{-2}
R_{lem}	Emitted longwave radiation	W m^{-2}
ε	Surface emissivity	(-)
σ	Stefan-Boltzmann constant	W m^{-2}K^{-4}
T_s	Surface temperature	K
R_{sdwn}	Down-welling shortwave	W m^{-2}
R_{ldwn}	Down-welling longwave	W m^{-2}
R_{sref}	Reflected shortwave	W m^{-2}
α	Surface albedo	(-)
m	Aerodynamic conductance to heat transport	(m/s)
ε 31	Spectral emissivity for wave-length of 11 μm	(-)
ε 32	Spectral emissivity for wave-length of 12 μm	(-)
BADAM	Ameriflux dataset	(-)
TERRA	NASA scientific research satellite	(-)
NATT	North Australian Tropical Transect	(-)

SI2. Comparison table of plot-scale LST with landscape LST using landscape and plot-scale ε

SI3. Emissivity estimation at Howards spring and positive $T_s - T_a$

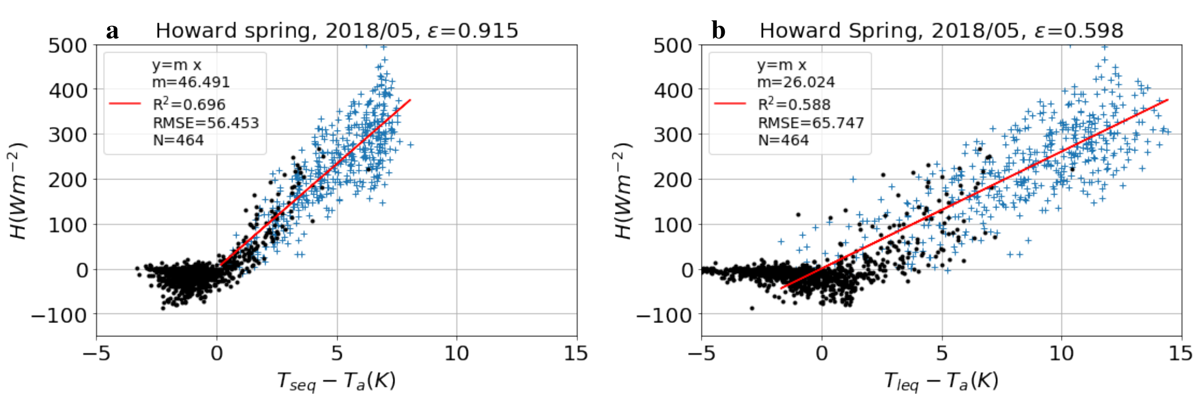

Figure 8. $Hand\Delta T$ plots at Howards Spring with optimised emissivity

Sites	Landscape-scale ε					Plot-scale ε					
	ε	seq		leq		seq			leq		
		R^2	bias	R^2	bias	opt ε	R^2	bias	opt ε	R^2	bias
SP	0.974	0.80	-3.67	0.81	-4.61	0.96	0.81	-3.0	0.85	0.82	-1.91
AS	0.974	0.93	-4.78	0.93	-6.31	0.96	0.93	-3.4	0.82	0.93	-1.92
TT	0.974	0.55	-6.76	0.57	-8.30	0.95	0.58	-5.06	0.80	0.52	-4.02
HS	0.985	0.16	-8.89	0.16	-9.90	0.92	0.21	-4.78	0.6	0.22	-2.47
LF	0.985	0.40	-10.0	0.41	-11.0	0.92	0.40	-4.41	0.6	0.41	-2.57
AR	0.985	0.18	-2.61	0.27	-3.51	0.997	0.23	-2.93	0.96	0.252	-2.98
DU	0.985	0.80	-3.67	0.81	-4.61	0.99	0.428	-3.682	0.985	0.425	-3.926
TUM	0.983	0.82	-2.27	0.84	-2.10	0.99	0.89	0.99	0.97	0.89	1.93
BR	0.983	0.937	0.525	0.937	-0.195	0.98	0.917	1.87	0.82	0.895	2.72
YA	0.974	0.855	-2.081	0.855	-3.45	0.97	0.522	-4.517	0.93	0.793	-0.582

Table 4. Comparison of plot-scale LST with landscape-scale daytime LST (MODIS, MODA001) at TERRA daily time of pass. Plot scale LST is obtained using landscape-scale emissivity (MODIS ε) and plot-scale emissivity (Optimum ε) at study sites. The reported plot-scale emissivity are median values and landscape emissivity are MODIS based. Bias is defined as mean of $T_s - T_{MODIS}$, R^2 is coefficient of determination between plot-scale LST in comparison to landscape-scale LST. The site acronyms can be found in Table 2

SI4. T_s sensitivity to ε at Alice spring and Tumbarumba

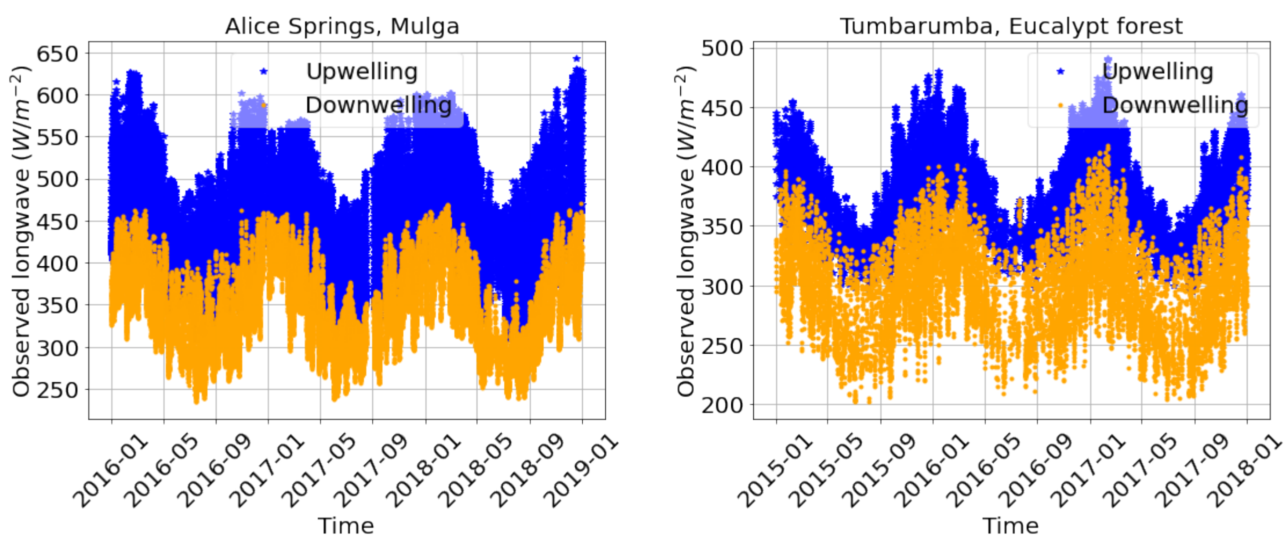

(a) Alice Springs

(b) Tumbarumba

Figure 9. Measured up-welling and down-welling longwave timeseries

In general, the broadband emissivity range for a land cover can vary between 0.87 to 0.98[?]. The noontime measured longwave for two contrasting landcover types (semi-arid mulga, tropical savanna woodland) are used to quantify the sensitivity of LST to emissivity as shown in Fig. (10).

SI5.RMSE and Epsilon

SI6.Energy imbalance and observed fluxes

SI7.H and intercept

SI7.Uncertainity and intercept

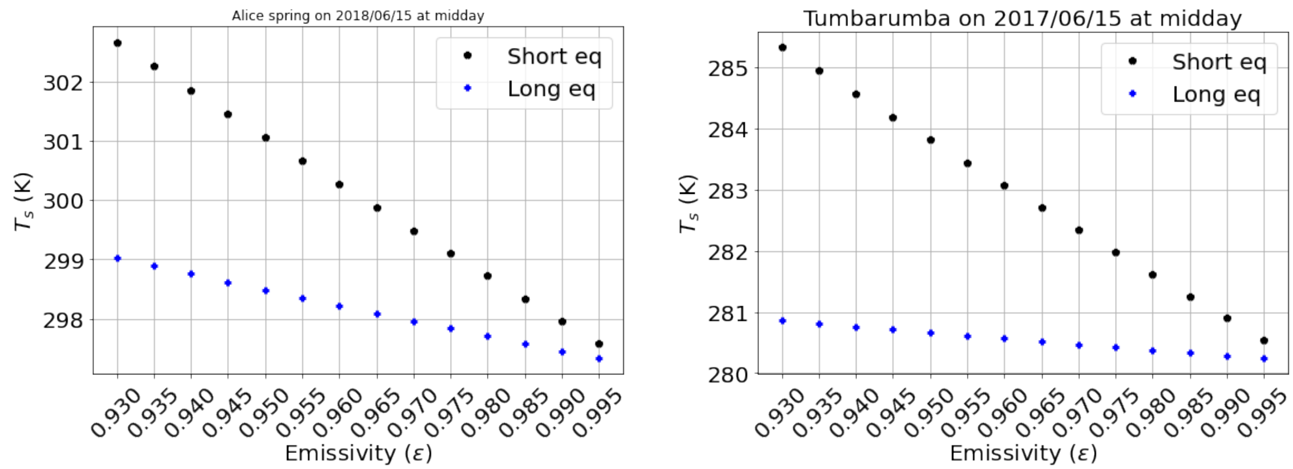

(a) **(b)**

Figure 10. Sensitivity of LST estimated using two equations to the range of Broadband emissivity The black dots and blue Stars depicts LST using simplified (Eq. 11) and complete (Eq. (6). Midday longwave measurement for 15June, 2016 at Alice Springs and Tumbarumba is used

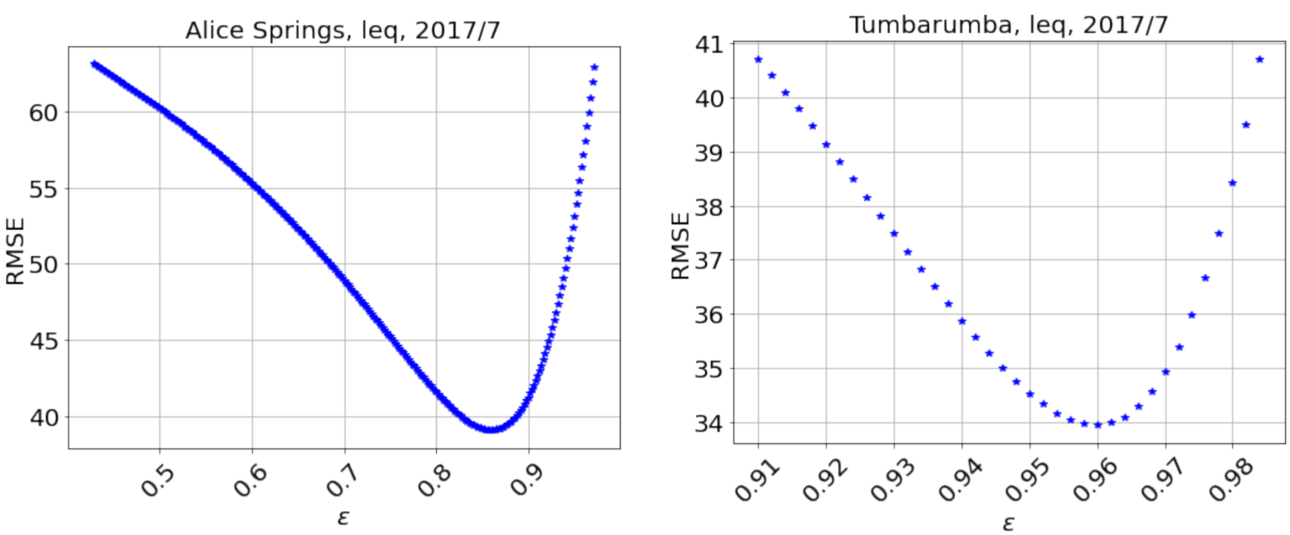

(a) Alice Springs

(b) Tumbarumba

Figure 11. RMSE and emissivity curve

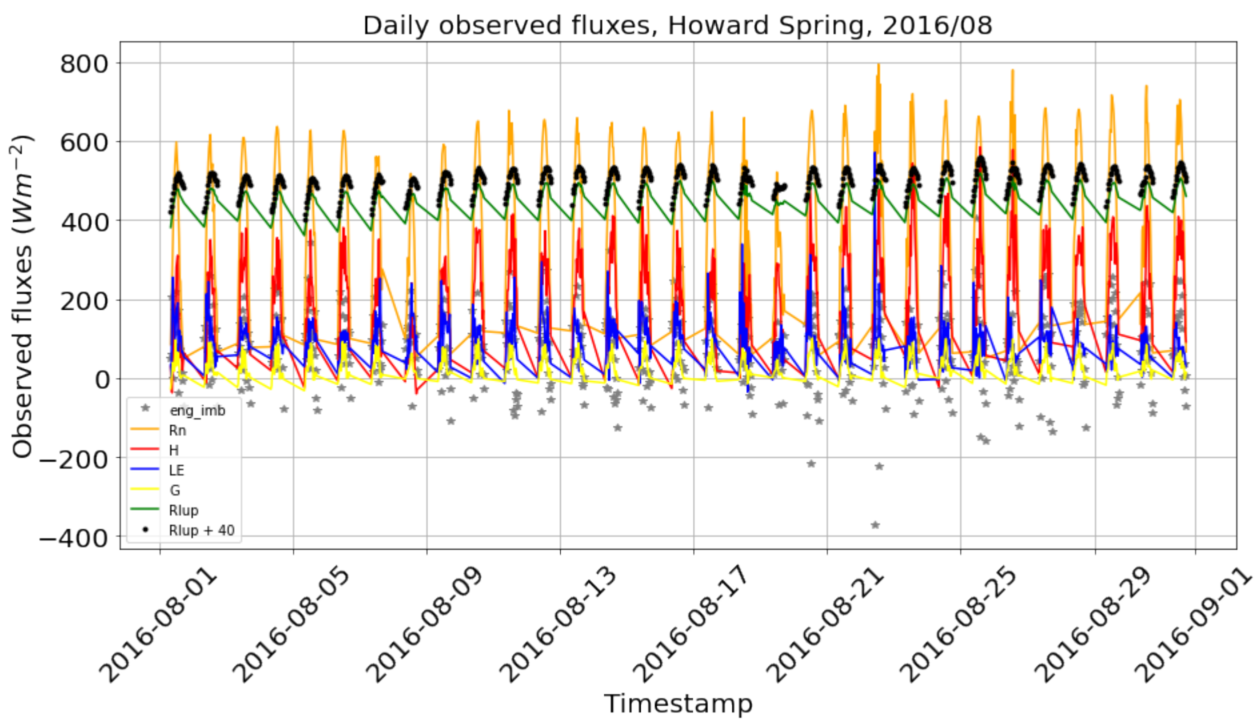

Figure 12. Measured fluxes and estimated energy imbalance at Howard springs for 2016/08

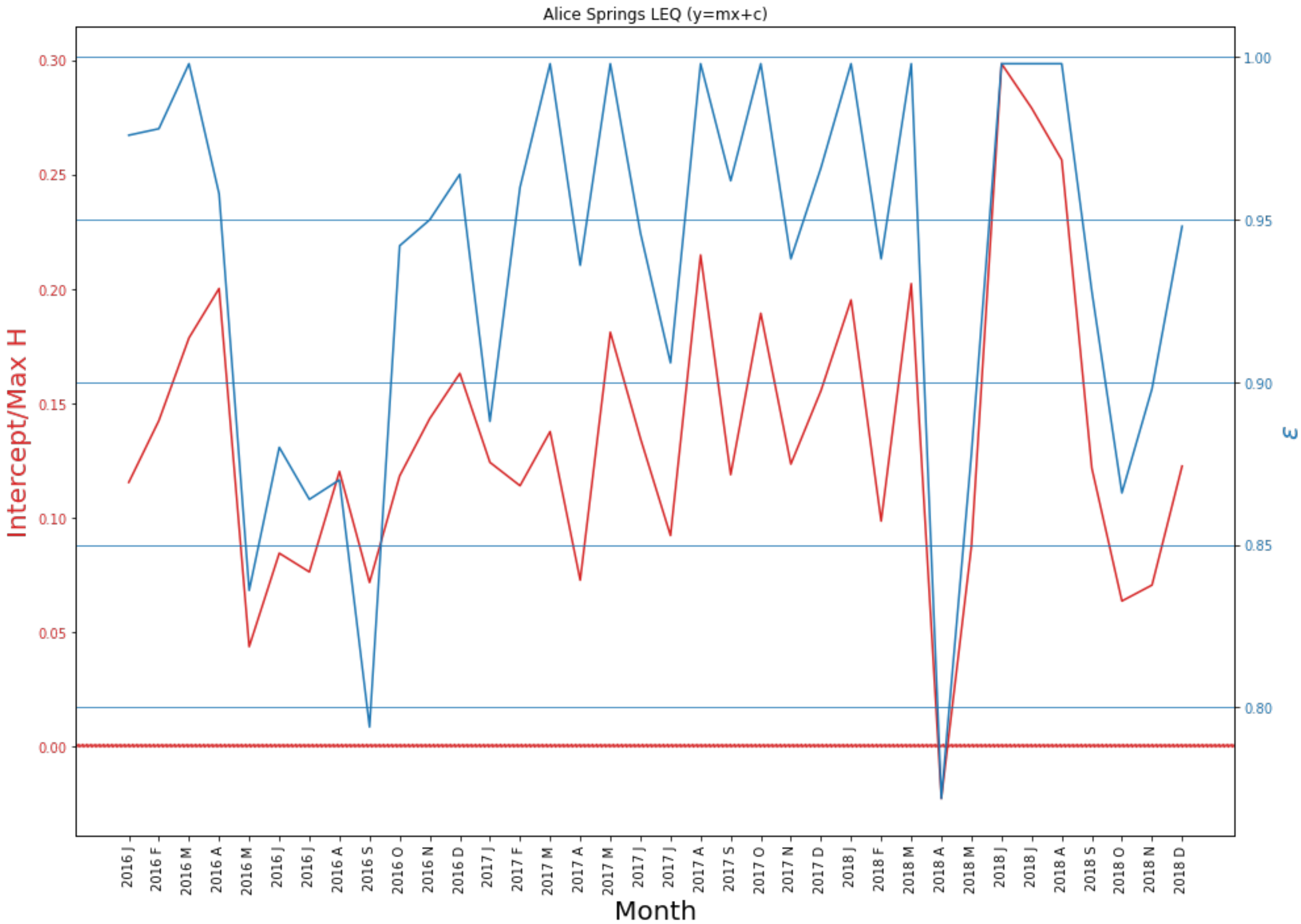

Figure 13. Monthly H ΔT plots showing offset at ΔT=0 **(a)** using simplified equation (Eq. 11). **(b)** using complete equation (Eq. 6)(c). Estimated intercept (c)for each month using $H = m(T_s - T_a) + c$. Red line is intercept and blue line shows monthly ε obtained by minimising RMSE at Alice Springs (2016 - 2018).

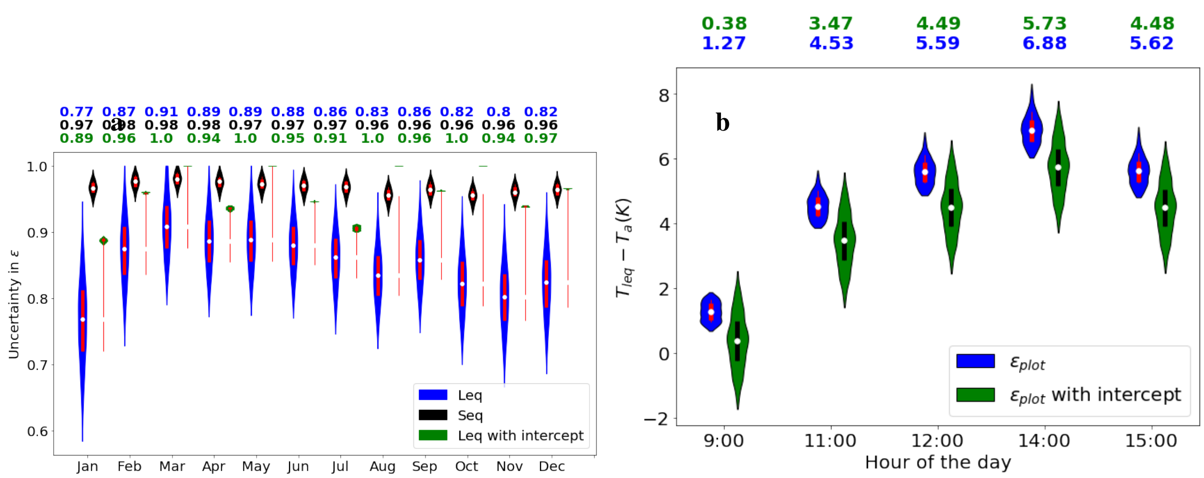

Figure 14. Uncertainity in plot-scale ε using long equation with and without intercept and hourly $T_s - T_a$